



# Ammonia emissions from a grazed field estimated by miniDOAS measurements and inverse dispersion modelling

Michael Bell<sup>1</sup>, Chris Flechard<sup>1</sup>, Yannick Fauvel<sup>1</sup>, Christoph Häni<sup>2</sup>, Jörg Sintermann<sup>3,a</sup>, Markus Jocher<sup>3</sup>, Harald Menzi<sup>4</sup>, Arjan Hensen<sup>5</sup>, and Albrecht Neftel<sup>3,b</sup>

<sup>1</sup>INRA, Agrocampus Ouest, UMR 1069 SAS, Rennes, France

<sup>2</sup>School of Agricultural, Forest and Food Sciences, Bern University of Applied Sciences, 3052 Zollikofen, Switzerland

<sup>3</sup>Agroscope, Institute for Sustainability Science, Zürich, Switzerland

<sup>4</sup>Federal Research Station Agroscope, Inst. For Livestock Sciences, 1725 Posieux, Switzerland

<sup>5</sup>Energy research Centre of the Netherlands (ECN), Petten, the Netherlands

<sup>a</sup>now at: AWEL, Zürich, Switzerland

<sup>b</sup>now at: Neftel Research Expertise, 3033 Wohlen b. Bern, Switzerland

Correspondence to: Michael Bell (michael.bell@inra.fr)

Received: 19 October 2016 – Discussion started: 9 December 2016

Revised: 11 April 2017 – Accepted: 13 April 2017 – Published: 29 May 2017

**Abstract.** Ammonia (NH<sub>3</sub>) fluxes were estimated from a field being grazed by dairy cattle during spring by applying a backward Lagrangian stochastic model (bLS) model combined with horizontal concentration gradients measured across the field. Continuous concentration measurements at field boundaries were made by open-path miniDOAS (differential optical absorption spectroscopy) instruments while the cattle were present and for 6 subsequent days. The deposition of emitted NH<sub>3</sub> to “clean” patches on the field was also simulated, allowing both “net” and “gross” emission estimates, where the dry deposition velocity ( $v_d$ ) was predicted by a canopy resistance ( $R_c$ ) model developed from local NH<sub>3</sub> flux and meteorological measurements. Estimated emissions peaked during grazing and decreased after the cattle had left the field, while control on emissions was observed from covariance with temperature, wind speed and humidity and wetness measurements made on the field, revealing a diurnal emission profile. Large concentration differences were observed between downwind receptors, due to spatially heterogeneous emission patterns. This was likely caused by uneven cattle distribution and a low grazing density, where “hotspots” of emissions would arise as the cattle grouped in certain areas, such as around the water trough. The spatial complexity was accounted for by separating the model source area into sub-sections and optimising individual source area coefficients to measured concentrations. The

background concentration was the greatest source of uncertainty, and based on a sensitivity/uncertainty analysis the overall uncertainty associated with derived emission factors from this study is at least 30–40 %.

Emission factors can be expressed as  $6 \pm 2 \text{ g NH}_3 \text{ cow}^{-1} \text{ day}^{-1}$ , or  $9 \pm 3 \%$  of excreted urine-N emitted as NH<sub>3</sub>, when deposition is not simulated and  $7 \pm 2 \text{ g NH}_3 \text{ cow}^{-1} \text{ day}^{-1}$ , or  $10 \pm 3 \%$  of excreted urine-N emitted as NH<sub>3</sub>, when deposition is included in the gross emission model. The results suggest that around  $14 \pm 4 \%$  of emitted NH<sub>3</sub> was deposited to patches within the field that were not affected by urine or dung.

## 1 Introduction

Over 90 % of anthropogenic ammonia (NH<sub>3</sub>) emissions in Europe have agricultural sources (Erisman et al., 2008; Reidy et al., 2008; Hertel et al., 2011), of which 70–90 % have been estimated to be produced by livestock (Pain et al., 1998; Hutchings et al., 2001). In addition to decreasing nitrogen efficiency for farming systems, the volatilisation of NH<sub>3</sub> from agricultural areas is a principal factor in the formation of fine-fraction secondary aerosols due to its reactions with nitric and sulfuric acids in the atmosphere and upon deposition is linked to acidification and eutrophication of natural

ecosystems (Sutton et al., 2011). Following the application of urine and dung to the soil surface by grazing livestock, urea is microbially converted to  $\text{NH}_3$  which is volatilised at rates which vary extensively depending on soil and canopy layer properties, weather and culture conditions (Laubach et al., 2013a). It has been estimated that 75–90 % of the N ingested by a grazing cow is metabolised inefficiently and returned by excreta to the grazing paddocks, of which over 70 % is returned as urine (Whitehead, 1995; Zaman et al., 2009).  $\text{NH}_3$  emissions have been measured from cattle urine patches at the ratio of 7–25.7 % of excreted urine nitrogen (N) for grazed pastures (Jarvis et al., 1989; Ryden et al., 1987; Laubach et al., 2012, 2013a), and measurements from sheep urine patches in summer–winter experiments have suggested emissions which represent 12.2–22.2 % of excreted urine-N (Sherlock and Goh, 1984).

Methods for estimating emissions from grazed pastures include micrometeorological methods, where profiles of concentration and wind speed are measured at one or more points downwind from the source, allowing fluxes to be calculated using the theory of turbulent transport in the atmospheric surface layer (Laubach et al., 2012). Dynamic chambers or movable wind tunnels may be used to estimate emissions from simulated grazing in the laboratory or the field (Sommer et al., 2001). However enclosure measurements may not always be representative of emissions at the field scale (Genermont and Cellier, 1997; Sintermann et al., 2012). The inverse dispersion method concerns the inferring of the atmospheric emission rate ( $Q$ ) of localised gas sources from the excess concentration ( $\Delta C$ ) they cause above background, by modelling the  $\Delta C/Q$  relationship for a given source-receptor configuration and meteorological state (Flesch et al., 2004, 2014).

The local dry deposition of  $\text{NH}_3$  within the grazed field is an important consideration, as in contrast to other pollutants a significant proportion may be deposited locally (e.g. Loubet et al., 2009). The proportion of deposited  $\text{NH}_3$  is sensitive to multiple parameters, including the source height, wind speed, atmospheric stability, land cover type and the numerous specific surface parameters therein (e.g. Sutton et al., 1993). This leads to modelling results that vary widely, with local recapture ranging from 2 to 60 % within 2 km from the source (Loubet et al., 2006; Asman et al., 1998). Accordingly, the modelling of  $\text{NH}_3$  deposition can be a challenging undertaking, with models ranging from simple steady-state canopy resistance models to dynamic, bi-directional, multi-layer and multi-process chemical species schemes (Flechar et al., 2013). Local-scale deposition models may ignore the wet deposition process, as dry deposition is most likely the dominant deposition mechanism near sources (Loubet et al., 2009).

In this study, a bLS (backward Lagrangian stochastic) dispersion model with a coupled dry deposition scheme has been applied to estimate the  $\text{NH}_3$  emissions from a field being grazed by dairy cows, using the horizontal concentra-

tion gradients measured across the field by three open-path miniDOAS (differential optical absorption spectroscopy) instruments (Sintermann et al., 2016; Volten et al., 2012). The open-path measurement system is of considerable benefit, as most techniques to measure atmospheric  $\text{NH}_3$  are sampling techniques and therefore involve inlet contact with the highly adhesive  $\text{NH}_3$ , which may slow response times and lead to interaction with water molecules and interference by ammonium aerosols dissociating on tubes or filters (e.g. von Bobrutski et al., 2010). The miniDOAS system is a comparatively interference-free measurement technique, since it utilises the wavelength-dependent UV-light absorption of  $\text{NH}_3$  over an open light path. The system also has capacity for long-term, fast-response, continuous measurements and a broad measurement path which makes the miniDOAS a well-suited concentration receptor for monitoring the fluctuations in  $\text{NH}_3$  concentrations across field boundaries.

The objectives of our study were (1) to evaluate the  $\text{NH}_3$  emissions from cattle grazing using the bLS dispersion technique and contribute towards an emission factor, as there is a limited number of existing measurements, (2) to simulate the degree of redeposition that occurs within the field, and (3) to evaluate the application of the bLS technique and the miniDOAS measurement system to derive  $\text{NH}_3$  fluxes from agricultural diffuse sources such as grazing. It was assumed that emission estimates would be insensitive to irregular cattle distribution and excretion patterns. The measurement of concentration gradients across grazed fields is challenging, as downwind concentration levels may not rise far above background as is the case with stronger sources, such as applied slurry. Therefore, this is an exercise which requires precise and continuous measurements from two or more sensors to evaluate  $\Delta C$ . However, the method is also non-intrusive, not labour intensive and can provide continuous emission estimates over long or short time periods if the conditions and experimental design are in agreement.

## 2 Methods

### 2.1 Site description and experimental design

The experiments were conducted from 18 to 29 May 2015 on a rectangular grazing pasture of about two hectares at the INRA-Méjusseume dairy research experimental farm in NW France (48°07'01.3" N 1°47'50.5" W). The site was flat and benefited from a lack of wind-disturbing elements within 100 m of the field boundaries (e.g. trees, buildings or other protruding elements). The cattle were not given additional feed to supplement grazing (mixed grass sward rich in *Lolium perenne*). The field had been previously grazed 1 month prior (16–27 April) to the beginning of the experiment, and mineral fertiliser had been applied on 31 March. During measurement Period 1, 25 cows were grazing within the south-western section of the field (area D, Fig. 1) from

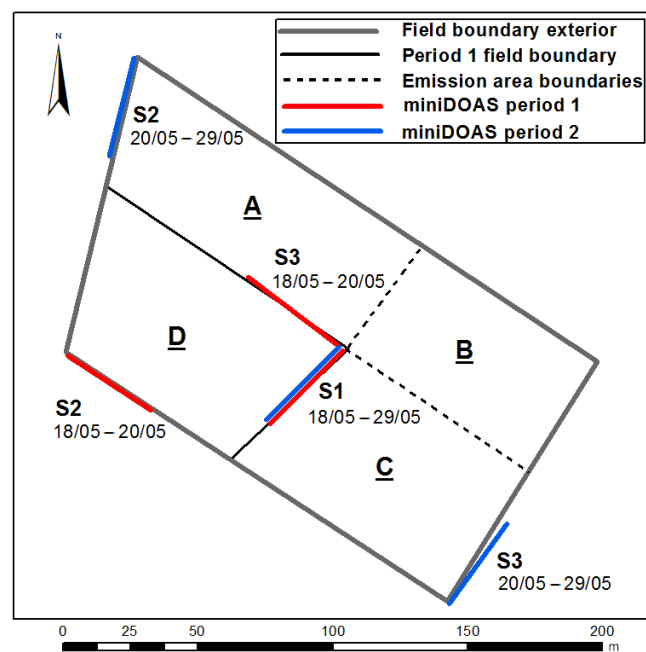


**Figure 1.** Map of the grazed field showing positions of the three miniDOAS open-path measurement systems. During Period 1 (18–20 May) 25 cattle were fenced within the SW field section (area D). During Period 2 (20–29 May) the internal field boundaries were removed so that the cattle could graze the whole field. Later, for the attribution of emissions across the field, emission area quadrants were allocated, marked A–D. There were no physical barriers between the emission areas during Period 2.

08:00 18 May–15:00 20 May 2015 UTC (28 h grazing), with three sets of miniDOAS open-path sensors being placed along the northern, western and eastern boundaries. The miniDOAS sensors were placed to optimise the measurement of  $\Delta C$  across the field after reviewing the wind directions forecast for the week ahead. The miniDOAS sensors have been given the names S1, S2 and S3, where the S2 sensor was placed upwind of the grazed field while the S1 and S3 sensors were placed at downwind locations. During Period 2, the whole field (areas A, B, C, D) was opened for 44 grazing cattle, with the cattle present on the field from 10:00 20 May–05:00 23 May (60 h grazing), while the miniDOAS sensors were left in place to measure residual emissions from 23 to 29 May. The cattle were removed from the field for milking during both periods for roughly 1 hour twice per day. As the field area during Period 2 was much larger, the S2 and S3 miniDOAS sensors were moved to the north-western and south-eastern field boundaries respectively, leaving the three miniDOAS paths in line with a NW–SE transect of the field (Fig. 1). The grazing densities during Period 1 and 2 were 44 and 22 cattle  $\text{ha}^{-1}$  respectively.

## 2.2 Ammonia measurements

The DOAS technique is based upon the wavelength-dependent absorption of light over a specified light path. The miniDOAS instruments offer greater portability and a lower cost relative to prior DOAS instruments (Volten et al., 2012). The broadband and narrowband extinction of UV light (equal to absorption + scattering) is measured across the light path, and the concentration of different trace gases is determined by their respective absorption spectra (details in Sintermann et al., 2016). In the wavelength range used by the miniDOAS (204–230 nm) narrowband absorption is seen by  $\text{NH}_3$ , sulfur dioxide ( $\text{SO}_2$ ), and nitrogen oxide ( $\text{NO}$ ), while other absorbers with broader absorption features are eliminated by high-pass filtering. The systems were calibrated prior to the field experiment using a flow cell in the miniDOAS light path with a high-concentration  $\text{NH}_3$  gas standard; in addition, the cell's outlet flow was checked by wet chemical impinger samples (two in a row) and photometric  $\text{NH}_3$  determination. Reference spectra ( $I_{\text{ref}}$ , see Sintermann et al., 2016) were determined for each instrument at the field site 1 week prior to the grazing experiment, where the three miniDOAS systems were configured to measure in parallel (measuring concentrations across the same open path). In order to provide the absolute concentration reference ( $c_{\text{ref}}$ , see Sintermann et al., 2016) for the miniDOAS, a transect of three sets of passive sampler (ALPHA) triplicates (Tang et al., 2001) were placed along the path length, giving a time-integrated  $c_{\text{ref}}$  measurement. The miniDOAS inter-comparison showed close agreement in the concentration levels between the three systems, where the coefficient of variation was 3.4 % (unpublished data). The random uncertainty of the miniDOAS measurements was determined to be 1.4 % of the concentration levels; however, it was not lower than  $0.2 \mu\text{g m}^{-2} \text{s}^{-1}$  (Sintermann et al., 2016). Since the initial miniDOAS publication (Sintermann et al., 2016) the calibration procedure has been revised to correct a gas standard error in the conversion from ppm to  $\mu\text{g m}^{-3}$ . The corrected measurements presented in this study are a factor of 1.16 higher relative to the  $\text{NH}_3$  concentrations presented by Sintermann et al. (2016).

To measure horizontal concentration gradients across the field, three miniDOAS instruments were placed strategically (based on the forecasted wind direction) at field boundaries at heights of 1.4 m above the ground, on stands drilled into the ground for stability. Retroreflectors were set 37 m away from each light source at the same height. A sensor placed upwind of the field would measure the background concentration ( $C_b$ ), which can be subtracted from the downwind concentration measurements ( $C$ ) to determine the horizontal concentration gradient or excess in concentration caused by emissions ( $\Delta C$ ). The miniDOAS concentration measurements were recorded at 1 min averaging intervals and later averaged to 30 min intervals for analysis.

### 2.3 Micrometeorological measurements

A three-dimensional ultrasonic anemometer (Gill WindMaster, Gill Instruments Limited, Lymington, UK) was mounted on an instrument tower at a 1.5 m height above the ground within a fenced-off section in the centre of the field. The sonic anemometer measured the three orthogonal wind components ( $u$ ,  $v$ ,  $w$  in  $\text{m s}^{-1}$ ) at a frequency of 20 Hz, along with a fast temperature measurement. Later the eddy covariance measurements were processed over 30 min averages, and the friction velocity ( $u^*$ ,  $\text{m s}^{-1}$ ), surface roughness ( $z_0$ , cm), Monin–Obukhov length ( $L$ , m), standard deviations of the rotated wind components ( $\sigma_u$ ,  $\sigma_v$ ,  $\sigma_w$ ), and resultant horizontal wind speed ( $u$ ,  $\text{m s}^{-1}$ ) and wind direction (wd) were computed. Correction factors were applied to fix a “bug” implicit within the Gill WindMaster instrument, as recommended by the manufacturer (Gill Instruments, 2016). The applied correction was a multiplication factor of 1.166 applied to positive vertical  $w$  wind axis measurements and a factor of 1.289 applied to negative  $w$  wind axis measurements.

Mounted on the instrument tower at 2 m height was a HMP45C sensor (Campbell Scientific, Loughborough, UK) which provided temperature ( $T$ ,  $^{\circ}\text{C}$ ) and relative humidity (RH, %) measurements. Leaf wetness (LW, % time wet) at canopy level was measured by a specialised conductivity sensor (Campbell Scientific, Loughborough, UK) placed 10 cm above the ground.

### 2.4 Dispersion modelling

The bLS type dispersion model is frequently applied for the computation of the inverse dispersion method (Flesch et al., 2004). Driven by measurements of the prevailing wind conditions, and with knowledge of the rise in concentration above background ( $\Delta C$ ) caused by an emitting source, the model can be applied to estimate the emission rate that best fits the measured concentration data. The measured wind statistics ( $\sigma_u$ ,  $\sigma_v$ ,  $\sigma_w$ ), atmospheric frictional velocity ( $u^*$ ), wind direction and surface roughness ( $z_0$ ) describe the wind flow characteristics, surface drag and buoyancy which enables the dispersion model to relate the downwind concentration fields to emissions from the source area. Within the horizontally homogeneous surface layer (height  $z < 100$  m, but above canopy level), the wind and turbulence measurements should be representative of the atmosphere over the entire site; thus, the sonic anemometer location is not critical. A condition of the bLS method states that the terrain should be tolerably homogeneous (Flesch et al., 2004); this criterion was met by the study site which consisted entirely of short grass (10–20 cm canopy height).

During bLS simulation the trajectories of thousands of fluid particles are calculated backwards in time from a reference point (concentration receptor) under the prevailing wind conditions. The locations where the trajectories intersect the ground (“touchdowns”) and the proportion of these

which fall within the source area ( $N_{\text{source}}$ ) are used to calculate  $\Delta C/Q$ , along with the associated vertical velocity ( $w_0$ ) of each touchdown (for details see Flesch et al., 1995, 2004).

The bLS-R model (Häni, 2016) is an inverse dispersion model that is based upon the backward Lagrangian stochastic dispersion theory described by Flesch et al. (1995, 2004); however, bLS-R has an additional function which computes the effect of dry deposition on gas concentrations. The bLS-R package provides functions to set up and execute the model within the R statistical software (R Core Team, 2016). Driven by the wind and turbulence inputs, for each time interval, the model calculates a dispersion coefficient  $D$  ( $\text{s m}^{-1}$ ) specific to the source–receptor geometry. The emission flux ( $Q$ ,  $\mu\text{g m}^{-2} \text{s}^{-1}$ ) may then be calculated from the measured rise in concentration above background ( $\Delta C$ ; Eq. 1).

$$Q = (\Delta C) \times D^{-1}, \quad (1)$$

where  $D$  is retrieved by the model from the number of source area interactions ( $N_{\text{source}}$ ) and the thousands of trajectories ( $N$ ) released backwards in time from the receptor locations (Eq. 2) and the vertical “touchdown velocities” at impact ( $w_0$ ) (for details see Flesch et al., 2004).

$$D = \frac{1}{N} \sum_{N_{\text{source}}} \left| \frac{2}{w_0} \right| \quad (2)$$

The following input data were applied in the bLS-R model as 30 min averages: wind direction, frictional velocity ( $u^*$ ), the standard deviations of the rotated wind vector components ( $\sigma_u$ ,  $\sigma_v$ ,  $\sigma_w$ ), and surface roughness ( $z_0$ ). The spatial dimensions of the grazed field source area and the miniDOAS receptors were also specified.

Independent concentration measurements and emission estimates were derived using the two downwind miniDOAS receptors (S1 and S3), which are compared throughout the paper, e.g. CS1, CS3 and QS1, QS3. All concentrations and fluxes are expressed in units of  $\text{NH}_3$ , e.g.  $\mu\text{g NH}_3 \text{ m}^{-3}$  and  $\mu\text{g NH}_3 \text{ m}^{-2} \text{ s}^{-1}$ .

### 2.5 Data filtering

The miniDOAS  $\text{NH}_3$  measurements were filtered to remove periods of high uncertainty, indicated by the standard error of the measurements. This filter only affected the S1 miniDOAS sensor, which was not fitted with an automatic alignment system to correct minor shifts in the light path between the lamp and reflector. After applying this filter 92 out of 430 half-hourly measurements were removed from the Period 2 S1 measurements (Period 1 measurements were unaffected).

Previous studies (Flesch et al., 2004; Harper et al., 2011) have applied  $u^*$  and Monin–Obukhov length ( $L$ ) filtering to remove emission estimates that do not meet given criteria ( $u^* > 0.15 \text{ m s}^{-1}$  and  $L > 10$  m). These criteria were established on the basis of an observed reduction in the accuracy of model predictions as  $u^*$  and  $L$  decrease (e.g. Flesch et al.,

2004; Gao et al., 2009). However, filtering out periods with low wind speeds and unstable stratification can be detrimental to emission estimates, often creating a bias to characterise certain sources under specific daytime or night-time conditions, whilst ignoring potentially valuable data that do not meet the criteria. This is a major limitation as we calculate average emissions from grazing cattle, where strong diurnal cycling is expected to occur (e.g. Laubach et al., 2013a). Flesch et al. (2014) developed alternate criteria for bLS data filtering, finding that (for their particular experiment) the  $u^*$  threshold could be reduced to  $0.05 \text{ m s}^{-1}$ , and, after finding no improvement after imposing a stability ( $L$ ) filter, introduced a supplementary vertical temperature gradient filter.

A filtering procedure was developed after assessing the standard error of emission estimates ( $\sigma_{Q/Q}$ ), which describes period-to-period fidelity and identifies “spiking” in model predictions caused by unsuitable input conditions, which do not conform to an underlying assumption of a horizontally homogenous surface layer (Flesch et al., 2014). It was found that a  $u^*$  threshold of  $0.1 \text{ m s}^{-1}$  was sufficient to remove the significant outliers, while retaining acceptable data coverage, although this filter was at times limiting for nocturnal (low wind) periods. A wind direction filter was applied to remove periods where miniDOAS sensors S1 and S3 were not downwind of the field area. This filter only affected sensor S3 during Period 2, where estimates were ignored if  $\text{wd} > 30$  and  $\text{wd} < 270$ .

## 2.6 Modelling of dry deposition within the source area

Downwind from a source of  $\text{NH}_3$ , local recapture will remove a certain fraction of emitted  $\text{NH}_3$  from the air. Therefore, the measured rise in concentration above background ( $\Delta C$ ) is a function of the source emission rate, atmospheric dispersion and the fraction that has been deposited. Within a field being grazed by dairy cattle, emissions of  $\text{NH}_3$  are expected from urine and dung patches, while deposition will occur on clean surfaces within and beyond the field. As we apply the bLS method to estimate emissions from the measured concentration gradient across the field ( $\Delta C$ ), we calculate the “net” flux constituting emissions from the field minus the fraction that has been deposited. However, if dry deposition is simulated in the dispersion model, the lost fraction of emissions due to deposition can be quantified, providing an estimate for the “gross” emissions from excretions during grazing.

The bLS-R model has a post-processing routine to simulate the effect of the dry deposition of  $\text{NH}_3$  on flux predictions. The exchange or deposition velocity ( $v_d$ ,  $\text{cm s}^{-1}$ ) is based upon a unidirectional resistance model approach, defined as the inverse of a sum of a series of resistances to deposition (Eq. 3, left side; Wesley and Hicks, 2000).

$$v_d = \frac{1}{R_a + R_b + R_c} = \frac{-F}{C}, \quad (3)$$

where  $R_a$  is the aerodynamic resistance to transfer through the turbulent surface layer for a certain reference height,  $R_b$  is the boundary layer resistance associated with the viscous quasi-laminar sublayer adjacent to the deposited surface and  $R_c$  is the canopy resistance representing the combined surface resistance accounting for stomatal and non-stomatal pathways to deposition (Flechar et al., 2013). It should be noted that  $R_a$  is implicit within the bLS-R calculations and does not need to be input into the model as a variable.

The unidirectional resistance model treatment is based upon strongly simplified assumptions regarding the near-ground  $\text{NH}_3$  concentrations and respective  $\text{NH}_3$  deposition flux, since the exchange of  $\text{NH}_3$  to ecosystems is bidirectional, involving many complex processes (Kruit et al., 2010; Fowler et al., 2009; Flechar et al., 2013).

The resistances to deposition  $R_a$  and  $R_b$  can be calculated using ultrasonic anemometer measurements and well-established models (Asman, 1998), while  $R_c$  is a composite term representing numerous physical barriers to deposition at the surface. To obtain local, field-scale estimates of  $R_c$ , two COTAG systems (conditional time-averaged gradient systems; Famulari et al., 2010) were operated at the centre of the grazed field for 1.5 years, allowing  $R_c$  to be estimated from calculations of  $R_a$  and  $R_b$  and time-integrated measurements of  $\text{NH}_3$  concentration ( $C$ ), flux ( $-F$ ) and  $v_d$  (Eq. 3). The COTAG measurements were filtered to remove grazing periods and periods up to 2 weeks after grazing had ended to ensure “clean” background conditions. Clear correlation was then observed between the time-integrated  $R_c$  estimates with the variables  $T$  ( $^{\circ}\text{C}$ ) and  $\text{RH}$  (%); thus, a double exponential equation was parameterised as follows to fit the data (Eq. 4, Fig. 2), with similar form to Flechar et al. (2010):

$$R_c = R_{c,\min} \times \exp^{\alpha \times (100 - \text{RH})} \times \exp^{\beta \times \text{Abs}(T)}. \quad (4)$$

A curve fitting procedure provided estimates of the parameters  $\alpha$ ,  $\beta$  and  $R_{c,\min}$  as  $0.013$  and  $0.015 \text{ }^{\circ}\text{C}^{-1}$  and  $10 \text{ s m}^{-1}$  respectively.

The deposition component of bLS-R operates on the assumption that the whole grazed field is acting as a homogenous surface for deposition; however, in reality urine and dung patches on the field are obviously hotspots of emissions and not  $\text{NH}_3$  sinks. The ratio of “clean canopy” where deposition may occur to “soiled canopy” is not known; thus, it is difficult to provide a true emission estimate including the effect of deposition. We can expect that the emission estimate without deposition ( $Q$ ) represents a net emission rate from the field, while, if we assume that the whole field behaves as homogenous sink, the emission rate including deposition will represent an upper limit of the gross emission estimate. The actual emission rate for a soiled field can be expected to fall somewhere between the net and upper gross estimates.

A means of addressing this issue with the heterogeneous canopy surface may be found in reviewing the  $R_c$  time series derived from the time-integrated COTAG concentration and

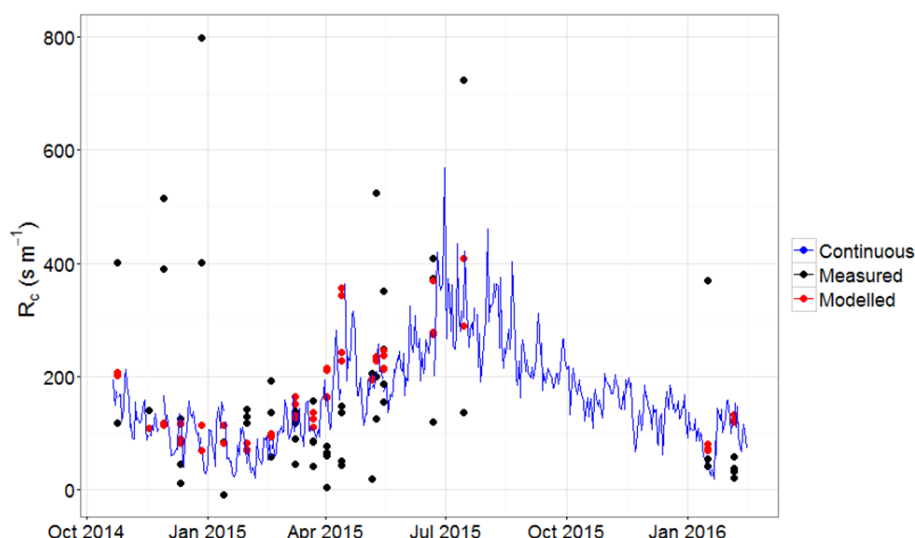


**Figure 2.** Time series of time-integrated COTAG  $R_c$  measurements and Eq. (4)  $R_c$  estimates. The blue line represents continuous  $R_c$  estimates calculated from the daily mean  $T$  and RH measurements at the field site. Black points are the measured  $R_c$  values from the COTAG systems, and the red points are the modelled  $R_c$  from the same time-integrated data.

flux measurements on the field, as  $v_d$  acts on the local vertical concentration gradient between surface and reference height, i.e. the flux is concentration gradient driven. At certain periods over the course of the year, cattle were brought onto the field for grazing, and shortly after the grazing periods had ended the  $\text{NH}_3$  flux would return back to the negative (deposition), and therefore  $R_c$  could be calculated. Averaging all the COTAG  $R_c$  calculations within 1 month following each grazing period gives an  $R_c$  value of  $260 \text{ s m}^{-1}$ , comparing this value with the average  $R_c$  where there had been no grazing on the field for at least 1 month ( $130 \text{ s m}^{-1}$ ). However, there was considerable scatter in the data, with standard deviations of 200 and  $40 \text{ s m}^{-1}$  for the post-grazing and clean periods respectively. Fertilisation of the field surface through grazing appears to have caused an increase in  $R_c$  of  $130 \text{ s m}^{-1}$ . This measured increase caused by excreted N to the field surface has been applied as an offset to the modelled  $R_c$  estimated by Eq. (4) and has been input into bLS-R. The bLS emission estimates without including deposition are referred to as  $Q$ , while the estimates including deposition and the  $R_c$  offset are referred to as  $Q_{\text{dep}}$ . Emission estimates including deposition but without the  $R_c$  offset are referred to as  $Q_{\text{depmax}}$ .

## 2.7 N excretion model

To contribute towards an emission factor for cattle grazing and to compare with literature values, it was necessary to express the emission estimates as a fraction of excreted N or urine-N. A nitrogen excretion model based on the Swiss feeding recommendations for dairy cows (Menzi et al., 2015; A. Muenger, personal communication, 2016) was applied to quantify the total N and urine-N excreted to the field dur-

ing both grazing periods, from the following set of inputs: (1) milk yield; (2) animal numbers, average weight and date after calving; (3) the net energy for lactation and crude protein content of the grass; and (4) the number of animals grazed and the duration of grazing on the experimental plot. The excretions per day were calculated as consumption minus retention in milk and animal growth. The share of N excreted in faeces and urine was calculated using regressions of fecal N digestibility derived from N balance studies (Bracher et al., 2011, 2012).

## 3 Results

### 3.1 Period 1 (18–20 May): grazing on SW paddock only

#### 3.1.1 Concentration measurements

The wind direction during Period 1 was consistently W–WSW (Fig. 3). Therefore, DOAS S2 was located upwind of the grazed SW paddock while S1 and S3 were situated downwind to the eastern and northeastern boundaries of the field respectively. Concentrations across the S2 path length would be expected to be low and near background, except during periods of very low wind speed, while any rise in concentration measured by S1 and S3 above S2 would show the influence of emissions from the field.

The upwind S2 concentration measurements reveal background concentrations of  $2\text{--}3 \mu\text{g m}^{-3}$  during times of steady W–SW winds, increasing slightly when wind speed was low. Concentration polar plots (Fig. 3) show the average concentrations measured as a function of wind speed and direction, where the influence of emissions from the grazed field is il-



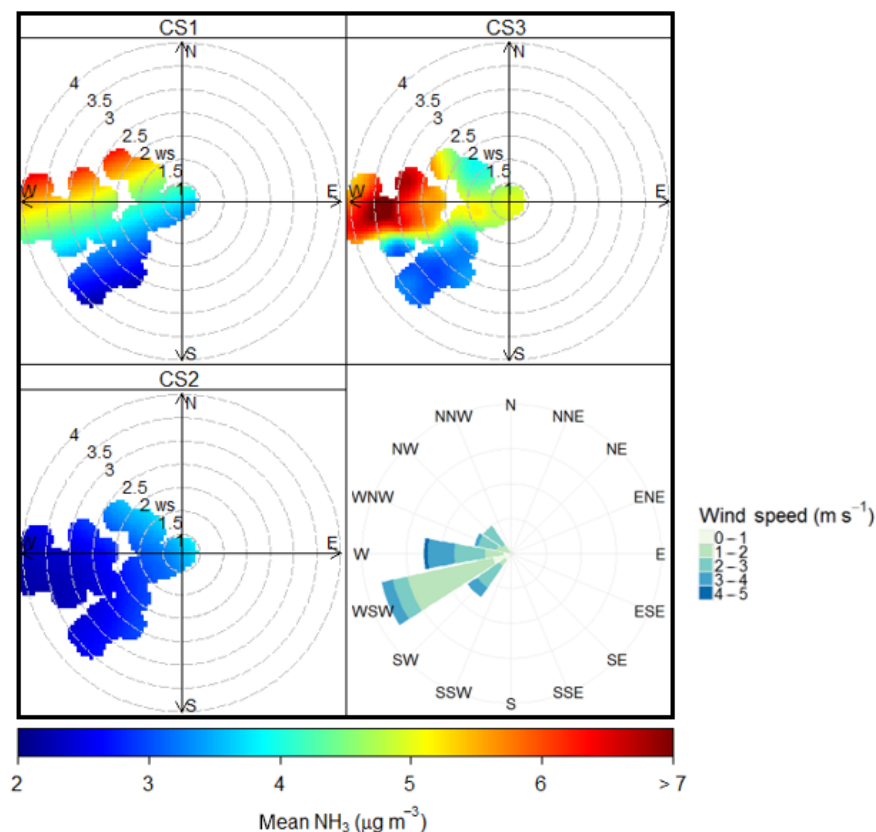


**Figure 3.** Polar plots showing averaged NH<sub>3</sub> concentrations (colour axis) as a function of wind speed (radial axis) and wind direction (cardinal direction) for each miniDOAS system, and a wind rose showing the prevailing wind direction, Period 1 (18–20 May). The concentration polar plots were produced using the openair R package (Carslaw et al., 2012).

illustrated by the increase in measured concentrations at downwind receptors S1 and S3 relative to S2 ( $C_b$ ).

Power failure led to a partial loss of measurements from miniDOAS S2, which are required to specify  $C_b$  for estimating emissions through bLS modelling. A significant linear regression was found between the measured background S2 concentration and wind speed ( $u$ , m s<sup>-1</sup>), temperature ( $T$ , °C) and relative humidity (RH, %):

$$C_b = 4.26 - 0.59u + 0.06T - 0.017RH, \quad r^2 = 0.5 \quad (5)$$

The wind direction remained consistent after the S2 power failed on 19 May; therefore, the empirical relationship (Eq. 5) was found to be suitable and was applied to estimate and extend S2 concentrations, as a proxy for  $C_b$ . The predicted S2 concentrations follow the measured S2 concentrations closely until the point of data loss on 19 May (Fig. 4a). This lends confidence to the rest of the  $C_b$  predictions used to fill the gap in the measurements, even though there is increased uncertainty associated with the last 15 h of emission estimates calculated from the predicted  $C_b$ , relative to periods where  $C_b$  was measured by the S2 sensor.

### 3.1.2 Field-scale emissions estimates

Overall there is very good agreement between the emission calculations from both downwind concentration datasets. The average emission rate calculated by bLS-R for the S3 measurements (QS3) is  $0.29 \mu\text{g m}^{-2} \text{s}^{-1}$ , while the QS1 average is  $0.27 \mu\text{g m}^{-2} \text{s}^{-1}$ . The modelled emission of NH<sub>3</sub> is low (generally below  $0.2 \mu\text{g m}^{-2} \text{s}^{-1}$ ) during the first 24 h, as the measured concentration gradient across the field was less than  $1 \mu\text{g m}^{-3}$ . As the cattle were introduced to the field on the first morning (18 May) it likely took some time for NH<sub>3</sub> to “build up” from the hydrolysis of excreted urea before significant emissions occurred. Downwind concentrations (CS1 and CS3) peaked during the next day (19 May), with peak emissions occurring at midday when there was a  $5\text{--}6 \mu\text{g m}^{-3}$  horizontal concentration gradient ( $\Delta C$ ) measured between the upwind and downwind receptors. The peak emission rate at this time was around  $1.1 \mu\text{g m}^{-2} \text{s}^{-1}$  for both downwind receptors. A decrease in the measured downwind concentrations occurred at 15:00 UTC, and an associated decrease in emissions is logically estimated for this time period. The decline in emissions follows 4.4 mm of rain during the day of 19 August, where the rainfall intensity peaked shortly after

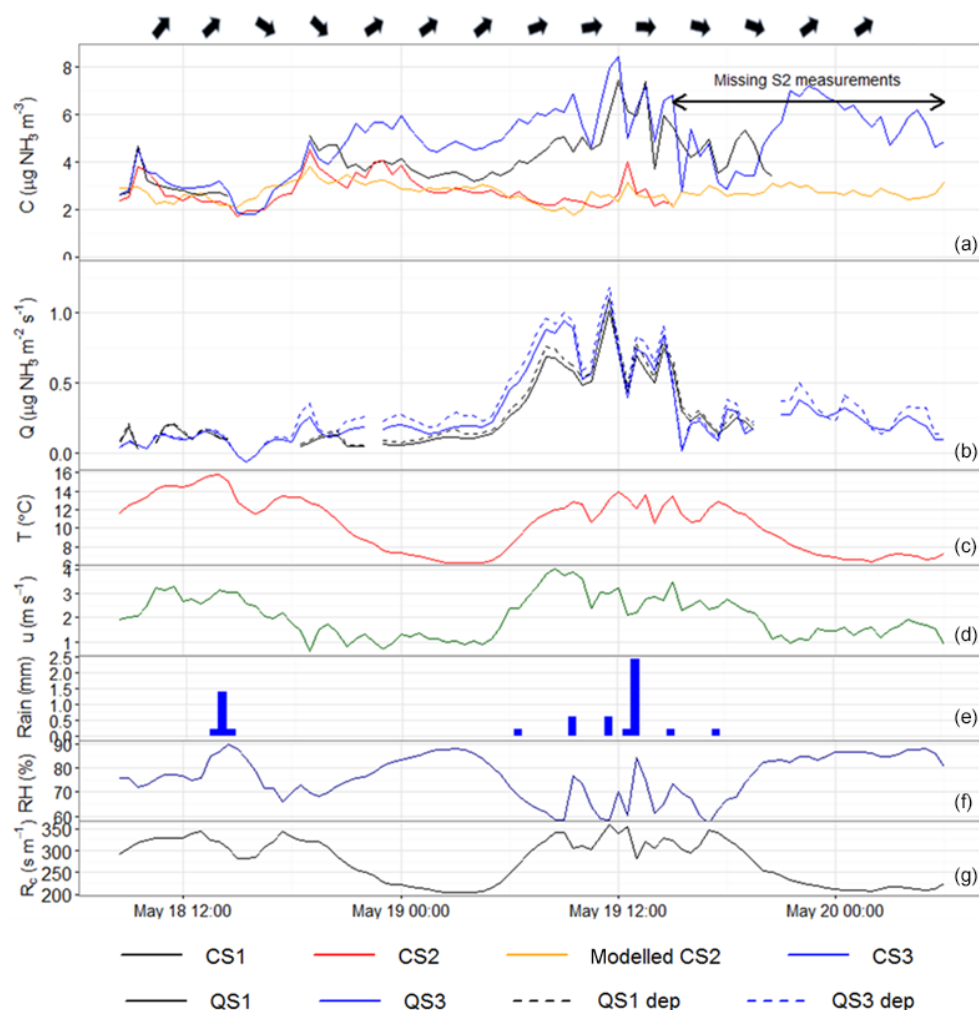


**Figure 4.** Time series of Period 1 DOAS concentration measurements (CS1, CS2, CS3 and modelled CS2 using Eq. 5, a) and bLS-R emission estimates ( $Q$  and  $Q_{\text{dep}}$  scenarios, second panel), with  $T$ ,  $u$ , rain, RH, and modelled  $R_c$  using Eq. (4) shown in the panels below. Wind direction arrows are set above the top panel to visualise changes over time. The cattle were present on the field for the full time period shown (08:00 18 May–15:00 20 May).

midday. In addition, the cattle were removed from the field at 15:00 UTC; therefore, the suspension of excretions to the field and the wet conditions are most likely the dominant factors driving the declining emissions. The LW sensor indicated that the canopy was wet (conductivity reading above baseline) for 84 % of Period 1 (Table 2).

Coinciding with the daytime peak in emissions and downwind concentrations were peaks in  $T$  and  $u$ , while RH reached a minimum (Fig. 4). During the night, emissions decreased to near 0, where RH reaches a maximum and  $T$  and  $u$  reach a minimum. The average  $Q_{\text{dep}}$  gross emission estimates are greater than the  $Q$  net emission estimates by 13–16 %.

### 3.2 Period 2 (20–29 May): grazing on the whole field

#### 3.2.1 Concentration measurements

Concentration measurements during Period 2 (20–29 May) revealed considerable differences between downwind receptors, where the average CS1 at the centre of the field was much greater than the average CS3 at the SE corner (Fig. 5), with period averages of 5.6 and 3.9  $\mu\text{g m}^{-3}$  respectively. This may be partially explained by the location of the receptors relative to the grazed field under the prevailing wind conditions. Sensor S1 was located in the centre of the field, with an upwind fetch of grazed field across a wider band of wind directions. Sensor S3 on the other hand is located at the SE field boundary and was more limited as a receptor for emissions under the prevailing northerly wind conditions. However, during NW wind directions where all sensors are in-



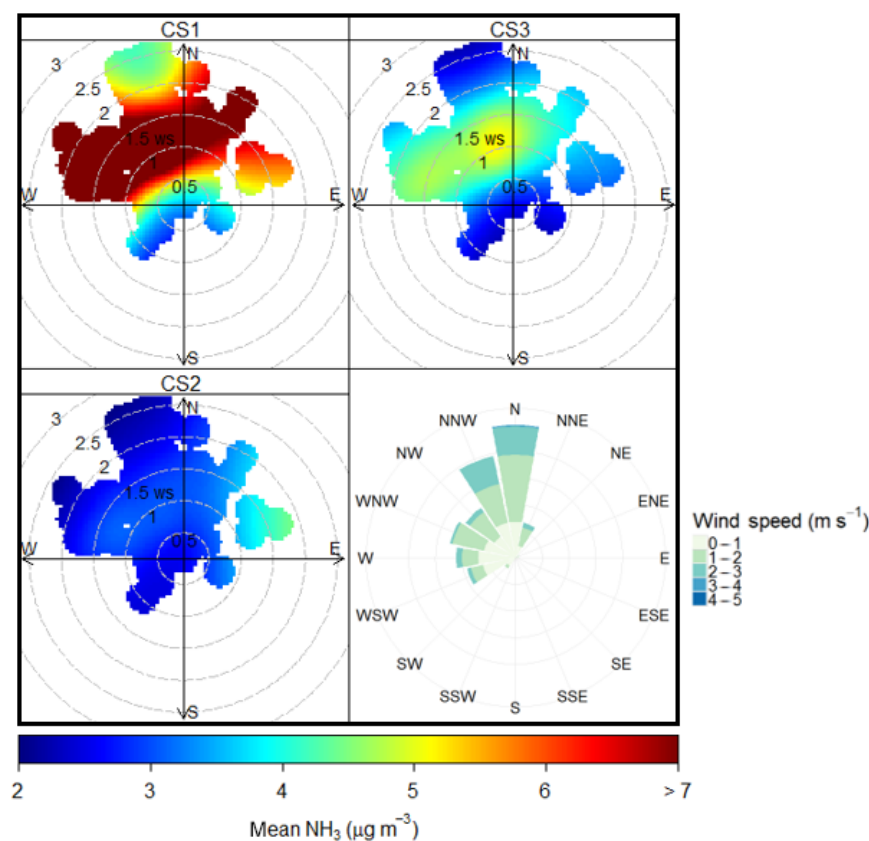


**Figure 5.** Polar plots showing averaged  $\text{NH}_3$  concentrations with wind speed and direction for each DOAS system, with a wind rose showing the prevailing wind directions, Period 2 (20–29 May).

line across a diagonal fetch of the field one would expect the S3 sensor to be measuring similar or higher concentrations relative to S1 at the centre (assuming homogenous emissions across the field), which is not the case. It is also important to note that the grazing density was about 50 % lower during Period 2 as the field was much larger.

Power failure led to significant data gaps from the S2 sensor and hence a loss of  $C_b$  measurements (Fig. 6). To fill the gaps a linear regression was applied between the measured S2 concentration and  $T$ ,  $u$ , and RH. However, there was considerable scatter in the data and the  $C_b$  prediction was much more uncertain than during Period 1.

$$C_b = 2.5 - 0.1u + 0.01T - 0.02RH, \quad r^2 = 0.1 \quad (6)$$

### 3.2.2 Field-scale emissions estimates

The average net emission rate ( $Q$ ) from the grazed field estimated using the S1 measurements was  $0.27 \mu\text{g m}^{-2} \text{s}^{-1}$ , while much lower emissions were estimated from the S3 measurements ( $0.12 \mu\text{g m}^{-2} \text{s}^{-1}$ ). Both estimates show a generally diurnal trend of peak emissions during the afternoon, similar to the trend observed during Period 1. However, there are gaps in  $QS1$  and  $QS3$  overnight due to data filtering as  $u^*$  drops below the defined threshold ( $0.1 \text{ m s}^{-1}$ ).

Peak emissions occurred on 22 May when the maximum concentration difference between upwind and downwind receptors was measured. Grazing of the field ended and the cattle left the field at 15:00 GMT on 23 May. After this point a generally decreasing trend in emissions is derived from the decreasing concentrations measured by S1 and S3. There is greater uncertainty attributed to the periods without active  $C_b$  measurements marked on Fig. 6.

Emission estimates from the bLS-R model were initially made on the assumption that emissions from the grazed field are spread equally (thus randomly) across a homogenous field. However a herd of cattle can be expected to move and disperse across the field in a generally non-random way, grouping together as they graze across the field rather than acting individually. Systematic effects of uneven cattle distribution within grazed pastures have been reported previously, impacting on bLS-derived mean gaseous emissions from grazing cattle (Laubach et al., 2013b). Our measurements during Period 2 certainly support spatial heterogeneity in emissions, with higher concentrations at the centre of the field (CS1) than at the SE corner (CS3) during periods in which the wind direction was from the NW. Had the emissions been spatially homogenous, as these emissions are taken up by the atmosphere and dispersed, an increase in

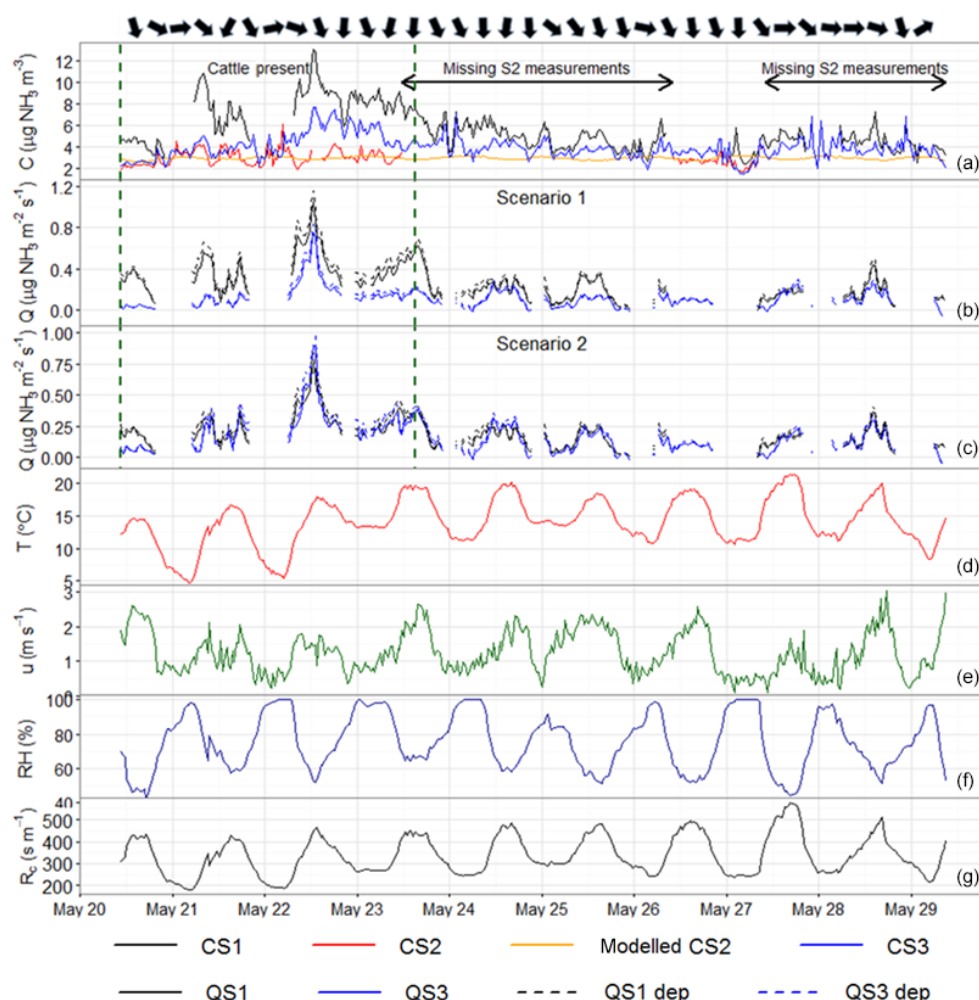


**Figure 6.** Time series of Period 2 DOAS concentration measurements (a) and bLS-R emission estimates (b, c; showing the  $Q$ , solid lines, and  $Q_{\text{dep}}$ , dashed lines, scenarios), with  $T$ ,  $u$ ,  $RH$ , and  $R_c$  (with  $130 \text{ s m}^{-1}$  offset) shown in the panels below. Panel (b) shows the Scenario 1 (homogenous field) emission estimates, while panel (c) contains the optimised Scenario 2 estimates using the heterogeneous source area coefficients given in Table 1. Periods with missing S2 background concentration measurements are annotated on panel (a) to highlight the higher uncertainty of these periods for emission estimates. Wind direction arrows are set above panel (a) to visualise changes over time. The dashed green lines on the panels (a–c) mark the 3-day time period where the cattle were grazing the field.

$\text{NH}_3$  concentration would have been measured with a distance downwind across the NW–SE transect of the field, causing higher concentrations at S3 compared to S1.

A second set of emission estimates (Fig. 6c) were produced after optimising the emission rates from four separate areas (A, B, C and D, Fig. 1) within the field to reproduce the observed concentrations at S1 and S3 on each measurement day. An excellent fit between  $QS1$  and  $QS3$  was achieved after running a numerical solver to minimise the squared error ( $e^2$ ) between them. The coefficients given in Table 1 are the result of the solver, describing the spatial changes in relative emission strength over time. The solver was executed with the following conditions: (1) the sum of the area coefficients must equal 1 and (2) no area coefficient can be below 0.075. The minimum value for any area coefficient ( $AC_{\text{min}}$ ) is a

parameter which describes the heterogeneity of emissions, where in this case it was assumed that each source area must contribute at least 30 % of the original (homogenous) value.

Henceforth the initial emission estimates calculated without applying emission area coefficients are referred to as Scenario 1 estimates, while the calculations involving heterogeneous emission area coefficients are referred to as Scenario 2 estimates. It is important to note that there can be more than one combination of coefficients to reconcile the  $QS1$  and  $QS3$  estimates; thus, these coefficients should not be taken as definite emission strengths for each area of the field. However, they do offer a rough guide to which sections had greater emissions relative to the others and confirm that emissions from the field were certainly not homogenous over the course of the grazing period. The large difference

**Table 1.** Series of emission coefficients obtained by numerical solving of the difference between  $QS1$  and  $QS3$  applied to individual emission areas to fit the bLS-R model to concentration measurements on each day. For a grazed field with homogenous emissions the emission coefficients for each area would be 0.25. Therefore, the emission coefficients offset the bias in emission estimates between the sensors  $S1$  and  $S3$  by adjusting to the heterogeneity in emissions across the field area.

Emission area	20 May	21 May	22 May	23 May	24 May	25 May	26 May	27 May	28 May	29 May
A	0.56	0.31	0.28	0.56	0.36	0.42	0.26	0.21	0.25	0.17
B	0.08	0.14	0.13	0.17	0.18	0.17	0.25	0.25	0.23	0.25
C	0.07	0.07	0.20	0.09	0.19	0.11	0.23	0.28	0.21	0.27
D	0.29	0.47	0.40	0.18	0.26	0.30	0.27	0.26	0.31	0.31

in Scenario 1  $QS1$  and  $QS3$  estimates may therefore be attributed to strong emissions in areas A and D, relative to C and B (Fig. 1, Table 1), which explains the high measured concentrations at sensor  $S1$  relative to  $S3$ . Emission area D represents the SW field which was grazed during Period 1; thus, high emissions from this area may have been a legacy effect left by continuing emissions from cattle excretions during Period 1. Emission area D also contained a water trough which was only 15–20 m away from the  $S1$  receptor, where cattle grouping was observed. Due to the combined effects of prior grazing within the SW field and grouping around the water trough, we can expect enhanced emissions within area D. The Scenario 2 (optimised)  $QS1$  and  $QS3$  estimates are similar (0.19 and  $0.16 \mu\text{g m}^{-2} \text{s}^{-1}$  respectively) and are believed to give a more realistic estimate of the true field-scale emission rates after accounting for spatial complexity. The data coverage for  $QS3$  (64 %) is greater than the  $QS1$  data coverage (59 %); hence, some differences between  $QS1$  and  $QS3$  can be expected even with perfect agreement. The  $Q$  estimates can be regarded as net emission rates for the grazed field, made without consideration of deposition to clean patches within the source area. The  $Q_{\text{dep}}$  estimates including the effect of deposition are 16 % higher (0.22 and  $0.19 \mu\text{g m}^{-2} \text{s}^{-1}$  for the Scenario 2  $S1$  and  $S3$  estimates respectively).

### 3.3 Derived emission factors

Grazing Period 1 took place within a SW section of the field with a smaller area ( $5600 \text{ m}^2$ ) than the whole field opened up for grazing Period 2 ( $19800 \text{ m}^2$ ). Although there were fewer cattle grazing during Period 1 (25), the grazing density was twice as high relative to Period 2. Therefore, the higher grazing density during Period 1 is consistent with the stronger emission estimates per unit area (Table 2). Emission factors (EFs) are given in Table 3 for Period 1 and 2. For both measurement periods, the  $S3$  sensor had greater data coverage than the  $S1$  sensor. Therefore, the  $S3$  emission estimates are more representative and are selected to derive EFs. Both grazing periods have produced similar emission factors of the order of  $6\text{--}7 \text{ g NH}_3 \text{ cow}^{-1} \text{ day}^{-1}$ , though there are considerable differences between the two periods in

**Table 2.** Summary table of measurement and modelling results.

	Period 1			Period 2		
	Scenario*	$S1$	$S3$	Scenario	$S1$	$S3$
$C - C_b$ ( $\mu\text{g NH}_3 \text{ m}^{-3}$ )		1.4	2.1		2.9	1.2
$Q$ ( $\mu\text{g NH}_3 \text{ m}^{-2} \text{s}^{-1}$ )		0.27	0.29	1	0.27	0.12
				2	0.19	0.16
$Q_{\text{dep}}$ ( $\mu\text{g NH}_3 \text{ m}^{-2} \text{s}^{-1}$ )		0.31	0.34	1	0.31	0.14
				2	0.22	0.19
$Q_{\text{depmax}}$ ( $\mu\text{g NH}_3 \text{ m}^{-2} \text{s}^{-1}$ )		0.33	0.38	1	0.33	0.14
				2	0.24	0.2
$T$ ( $^{\circ}\text{C}$ )		10			14	
$u$ ( $\text{m s}^{-1}$ )		2			1.2	
RH (%)		77			76	
Total rain (mm)		4.4			0	
LW (% time wet)		84			40	
$R_c$ ( $\text{s m}^{-1}$ )	$Q_{\text{depmax}}$	145		$Q_{\text{depmax}}$	208	
	$Q_{\text{dep}}$	275		$Q_{\text{dep}}$	338	
$v_d$ ( $\text{mm s}^{-1}$ )	$Q_{\text{depmax}}$	4.4		$Q_{\text{depmax}}$	3.2	
	$Q_{\text{dep}}$	2.8		$Q_{\text{dep}}$	2.2	

\* Description of model scenarios:  $Q_{\text{dep}}$  is the bLS-R emission estimate including dry deposition, with an offset of  $130 \text{ s m}^{-1}$  applied to the  $R_c$  time series to account for the limiting of excreted  $\text{NH}_3$  to deposition.  $Q_{\text{depmax}}$  is the emission estimate without the offset applied to the  $R_c$  time series and is hence a maximum prediction of the gross emissions from the field. Period 2 emission estimates contain both the original Scenario 1 emission estimates assuming a homogenous field and the optimised Scenario 2 emission estimates using the area coefficients given in Table 1.

terms of weather conditions and grazing timeline. Period 1 was shorter in length and was characterised by steady SW–W winds, lower temperatures and wetter conditions relative to Period 2 (Table 2). Therefore, the lower temperatures and wetter conditions likely limited emissions (e.g. Flechard et al., 1999; Laubach et al., 2012; Mórning et al., 2016).

The duration of Period 1 was too short to fully capture tailing emissions; excretions to the field during Period 1 will have continued to emit  $\text{NH}_3$  during Period 2. Flux estimates are continued for 6 days after the cattle had left the field during Period 2, capturing residual emissions after grazing. The combined influences of weather conditions and experimental design and duration may therefore explain why a smaller fraction of excreted N and urine-N was emitted as  $\text{NH}_3$  during Period 1 relative to Period 2. The EFs derived from Pe-

**Table 3.** N excretion model inputs, results, and derived emission factors.

Model input	Value		Model output or emission	Scenario <sup>b</sup>	Value	
	Period 1	Period 2	Factor <sup>a</sup>		Period 1	Period 2
Animal numbers	25	44	N excretion total (kg)		11	40
Animal weight (kg)	650	650	N excretion urine (kg)		8	28
Days since calving	180	183	N excretion faeces (kg)		3	12
Milk yield (kg cow <sup>-1</sup> day <sup>-1</sup> )	21	22	EF (% total excreted N emitted as NH <sub>3</sub> )	<i>Q</i>	2.5	5.2
				<i>Q</i> <sub>dep</sub>	2.9	6
Grass sward: net energy for lactation (MJ kg DM <sup>-1</sup> )	6.4	6.4	EF (% total excreted urine-N emitted as NH <sub>3</sub> )	<i>Q</i>	2.9	8.9
				<i>Q</i> <sub>dep</sub>	4.2	10.4
Grass sward: crude protein content (g kg DM <sup>-1</sup> )	168	168	EF (g NH <sub>3</sub> cow <sup>-1</sup> day <sup>-1</sup> )	<i>Q</i>	5.7	6.2
				<i>Q</i> <sub>dep</sub>	6.5	7.2

<sup>a</sup> N excretion calculations are given as the herd total for each measurement period.  
<sup>b</sup> *Q* is the net emission rate derived without including deposition in the bLS-R simulation and *Q*<sub>dep</sub> is the gross bLS-R emission estimate including dry deposition, with an *R<sub>c</sub>* offset of 130 s m<sup>-1</sup>. EFs are derived from the S3 flux estimates due to better data coverage during both measurement periods, and Period 2 fluxes are derived from Scenario 2 estimates.

riod 2 fluxes may for these reasons be considered to be more representative of the total emissions from grazing, where emissions are estimated to be 6 and 7 g NH<sub>3</sub> cow<sup>-1</sup> day<sup>-1</sup> and 9 and 10 % excreted urine-N emitted as NH<sub>3</sub> for the *Q* and *Q*<sub>dep</sub> scenarios respectively. However, the greater uncertainty in Period 2 associated with missing *C<sub>b</sub>* measurements and heterogeneous emission patterns should be considered.

4 Discussion

4.1 Experimental design

Previous experiments to deduce surface–air fluxes by the bLS method have deployed sufficient measurement systems so that the problem to determine *C* and *C<sub>b</sub>* was mathematically over-determined, and the experiment was not dependent on a specific range of wind directions (e.g. Flesch et al., 2014). The configuration of the three miniDOAS sensors and the grazed field during Period 2 led to certain wind directions being unsuitable for emission estimates, while additional miniDOAS sensors placed at field boundaries would have been beneficial. However, the configuration of the miniDOAS sensors was optimised by using the weather forecast to predict the wind direction prior to the grazing experiment and placing the miniDOAS sensors accordingly.

It was originally hypothesised that the model could treat the field area as a spatially homogenous source, where emission estimates would show insensitivity to cattle grouping and excretion patterns within the field. This assumption seemed valid for the Period 1 emission estimates, where very good agreement was achieved in *C* and *Q* between the downwind receptors. The SW field grazed during Period 1 was

smaller than the whole field grazed during Period 2, and the wind direction was more consistent. This allowed the downwind and upwind receptors to capture the inflow and outflow concentrations and produce reliable emission estimates, while the grazing density was higher. During Period 2 the field was larger and the grazing density was 50 % lower, which led to some spatial and temporal emission “hotspots” caused by cattle grouping and/or excretions within certain areas, such as around the water trough. The S1 sensor was located very close to a hotspot of emissions at the centre and SW section of the field, while the S3 sensor was located next to an area (SE corner) which appears to have seen relatively little emissions. Because of this the model could not treat the field as a homogenous source area and reconcile emission estimates between downwind receptors, and source area differentiation (Table 1) was required. Clearly, there is a limitation in the application of the standard bLS method to estimate emissions from area sources which may not be treated as homogenous, such as pastures with a low grazing density. However, as the Period 2/Scenario 2 emission estimates demonstrate it may also be possible to account for this heterogeneity if more than one downwind concentration receptor is used and they are suitably located. Insensitivity to heterogeneous emissions has been demonstrated if concentration measurements are made at least twice as far downwind as the maximum distance between potential sources (Flesch et al., 2005). Therefore, had the miniDOAS sensors been placed differently to satisfy this criterion, it is possible that no source area optimisation would have been necessary to reconcile bLS emission estimates. On the other hand, as emissions from excretions to the grazed pasture were relatively weak, at a greater distance downwind from the field

the concentration rise above background may not be significant enough to evaluate the emissions.

Felber et al. (2015) applied corralling of grazing cattle into paddocks over a rotational grazing cycle to increase grazing density and placed GPS trackers on individual cattle to attribute eddy covariance methane fluxes using a footprint model. The Period 1 emission estimates demonstrate that a smaller paddock and higher grazing density can be a solution to the heterogeneous emissions problem; however,  $\text{NH}_3$  emissions from grazing cattle arise from excretions to the field surface and are not enteric, so GPS trackers on cattle may not track the  $\text{NH}_3$  emissions directly as they do for methane. In order to accurately attribute fluxes from grazed pastures there is a call to develop a method to track excretions spatially and temporally across a grazed field, potentially using visual observations or cameras and animal detection software. We did carry out visual observations of urination events during Period 1 (day time only), which described a fairly homogenous distribution (data not shown, A. Möring, personal communication, 2015). Unfortunately, observations could not be carried out during Period 2.

## 4.2 Uncertainty in field-scale emission estimates

### 4.2.1 Uncertainty in miniDOAS concentration measurements and dispersion model

The instrumental uncertainty associated with the miniDOAS concentration measurements was evaluated during the initial inter-comparison phase, where the systems were configured to measure in parallel. Very good agreement was observed between the analysers, with a slope of 1 and an intercept close to 0. Deviations between the S1, S2 and S3 analysers were minor, and the coefficient of variation between them was determined to be 3.4 % (unpublished data). Sintermann et al. (2016) have described this inter-comparison phase and the miniDOAS performance in detail; however, the authors compare only the miniDOAS sensors S2 and S3 as these sensors were fitted with all of the updated Swiss miniDOAS instrumental features discussed within that study.

Since the input data had been filtered to remove conditions which do not meet the established criteria ( $u^* < 0.1 \text{ m s}^{-1}$ ), and instrumental uncertainty associated with the concentration measurements is very low, the principal uncertainties are associated with the modelled results, principally the input variables which could not be measured directly, such as  $R_c$  and the predicted background concentration  $C_b$  used for gap filling.

The bLS dispersion model theory has been well validated in past experiments (e.g. Flesch et al., 2004; McGinn et al., 2009), however we can assume a general overall uncertainty based on evaluated performance by an ensemble of published trace gas release experiments. A review of 24 bLS tracer release assessments (Häni et al., 2016) found that the uncertainty is generally between 10 and 20 % for the bLS method.

### 4.2.2 Uncertainty in background concentration

The background concentration ( $C_b$ ) had to be predicted to “fill in” the gaps in the  $C_b$  measurements upwind of the field measured by miniDOAS sensor S2. Multiple regression equations (Eqs. 5, 6) were based on previous observations that background  $\text{NH}_3$  is dependent on wind speed, temperature and relative humidity (Flechard and Fowler, 1998), but nonetheless error is introduced due to differences between the predicted  $C_b$  and the actual  $C_b$ . The mean absolute error (MAE) between the measured and predicted  $C_b$  for Period 1 and 2 has been applied to offset to the predicted  $C_b$  time series input into the model to determine the limits (upper and lower) of emission estimates caused by this uncertainty. The MAE between the observed and predicted background concentrations during Period 1 was  $0.33 \mu\text{g m}^{-3}$ , while the percentage of data coverage (observed  $C_b$  measurements) was 67 %. Measurement Period 2 had a greater MAE between observed and predicted  $C_b$  ( $0.56 \mu\text{g m}^{-3}$ ; Table 4), as the multiple regression equation used to fill  $C_b$  measurement gaps did not give very accurate predictions (Eq. 6). Furthermore, the upwind sensor S2 was only active during 44 % of the measurement period; therefore, the Period 2 emission estimates are more sensitive to this uncertainty. The percent change in  $Q_{\text{dep}}$  to predicted  $C_b \pm \text{MAE}$  was much greater during Period 2 ( $\pm 31$  %) than Period 1 ( $\pm 5$  %).

### 4.2.3 Uncertainty in local dry deposition of field-emitted $\text{NH}_3$

The inclusion of dry deposition within the bLS-R model is intended to simulate the deposition of  $\text{NH}_3$  to the surface of clean grass patches within the grazed field. This process is described by a resistance model, and while the  $R_a$  and  $R_b$  components may be derived directly from eddy covariance measurements, as well as well-established models, the  $R_c$  component is empirical. In this case, the empirical  $R_c$  model (Eq. 4) was derived from a curve fitting exercise of time-integrated COTAG flux measurement to meteorological variables  $T$  and RH. The  $R_c$  model is based on a long (1.5 years) series of measurements taken from the field (deposition periods only), while the effect of soiled grass areas on  $R_c$  during grazing is also approximated using the  $130 \text{ s m}^{-1}$   $R_c$  offset within the  $Q_{\text{dep}}$  scenario. It is conceivable that there is significant error (up to 50 %) in estimating  $R_c$  by this method. The sensitivity of the bLS-R model to potential uncertainty within the  $R_c$  estimates has been evaluated, where the  $R_c$  time series has been varied by factors of plus and minus 50 %. The results of this sensitivity test are given in Table 4. The percent change in  $Q_{\text{dep}}$  after varying  $R_c$  by  $\pm 50$  % was  $-4$  and  $+12$  % for Period 1 and  $\pm 5$  % for Period 2.

While impact of this uncertainty on the absolute value for  $Q_{\text{dep}}$  is not very large, the change in  $Q_{\text{dep}}$  relative to  $Q$  is significant. The Period 2  $Q_{\text{dep}}$  uncertainty due to predicted  $R_c$  is  $\pm 5$  %; therefore, including deposition in the model has

**Table 4.** Sensitivity analysis of the percentage change of the bLS-R gross emission estimates ( $Q_{\text{dep}}$ ) to variation in predicted  $C_b$  and  $R_c$  as well as the source area coefficient parameter  $AC_{\text{min}}$ .

	Period 1	Period 2
$C_b$ data coverage (%)	67	44
$C_b$ MAE ( $\mu\text{g m}^{-3}$ )	0.33	0.56
% change $C_b \pm \text{MAE}^a$	−5 % +5 %	−31 % +31 %
% change $R_c \pm 20$ %	−2 % +3 %	−3 % +3 %
% change $R_c \pm 50$ %	−4 % +12 %	−5 % +5 %
% change $AC_{\text{min}} \pm 67$ % <sup>b</sup>	−	−9 % −1 %

<sup>a</sup> The predicted  $C_b$  time series input into the bLS-R model is varied by the Mean Absolute Error (MAE) between the measured and predicted  $C_b$ . The first value in all cases the percent (%) change + variation and the second the % change − variation.

<sup>b</sup> The percentage change in  $Q_{\text{dep}}$  is given after varying the source area coefficient parameter  $AC_{\text{min}}$  by 67 % ( $0.075 \pm 0.05$ ).

increased  $Q_{\text{dep}}$  above  $Q$  by  $16 \pm 6$  %. Alternatively, we can say that  $14 \pm 4$  % of  $\text{NH}_3$  emitted from excretions had been redeposited to clean patches on the field.

#### 4.2.4 Uncertainty associated with heterogeneous emission patterns

To address the resulting disparity between emission estimates from the downwind concentration receptors during Period 2, the emission area coefficients (Table 1) were applied to reconcile the independent emission estimates. This is a valid approach to describe emissions from the field as a whole, as sensor S1 was placed at the centre of the field near the strongest area of emissions, causing emissions to be over-estimated as a whole, while the field area around sensor S3 at the SE corner seems to have contributed very few emissions, hence causing an underestimation. However, as mentioned previously there are multiple configurations of source area coefficients which can reconcile  $QS1$  and  $QS3$ . Therefore, a sensitivity test has been carried out to evaluate the potential error in this method. The numerical solver which derives the source area coefficients contains a parameter assuming the maximum degree of heterogeneity for the field, where each source area cannot contribute less than a defined percentage to the overall emissions. This parameter ( $AC_{\text{min}}$ ) was varied to provide differing sets of source area coefficients, yet still reconciling the  $QS1$  and  $QS3$  emission estimates, which was a necessary precondition for the sensitivity test.  $AC_{\text{min}}$  was initially assumed be 0.075, 30 % of the value for a homogenous field (0.25), and this value was varied by  $\pm 67$  % (to 50 and 10 % of the homogenous value). The results of this sensitivity test are given in Table 4, where the percentage change in  $Q_{\text{dep}}$  after varying the parameter by +67 and −67 % was 9 and 1 respectively. The percentage change is greater after increasing  $AC_{\text{min}}$  because  $QS1$  and  $QS3$  cannot be reconciled as closely, whereas decreasing  $AC_{\text{min}}$  from 0.075 leads to very little change as the numerical solver can find very close

agreement. This suggests that emissions from excretions to the field are too heterogeneous to assume an  $AC_{\text{min}}$  value of 0.125 (50 % of homogenous value) and that the 1 % change in  $Q_{\text{dep}}$  after reducing  $AC_{\text{min}}$  to 0.025 (10 % of homogenous value) is more indicative of the uncertainty in the source area optimisation method.

The percent change in emission estimates was much more sensitive to uncertainty in predicted  $C_b$  than to uncertainty in  $R_c$  or  $AC_{\text{min}}$ . Therefore, we expect that the predicted  $C_b$  is the greatest source of error in derived fluxes from the grazed field.

#### 4.3 Temporal variability in estimated emissions

The estimated emissions show significant temporal variability during both measurement periods, typically with peak emissions occurring during the day and with few emissions occurring overnight. Similar diurnal profiles have been observed in  $\text{NH}_3$  emissions from cattle urine and dung patches (Laubach et al., 2012, 2013a) as well as from urine patch emission models (Móring et al., 2016). The mechanisms which limit nocturnal emissions can be summarised as (1) low wind speeds and stable conditions, which increases the aerodynamic transfer resistances between the soil or canopy layer and the atmosphere, (2) low temperatures which limit the hydrolysis of urea and affect  $\text{NH}_3$  and  $\text{NH}_4^+$  partitioning in solutions, and (3) dew formation on leaf surfaces which act as sinks for  $\text{NH}_3$ .

A longer temporal trend in emissions is observed during Period 1, with very few emissions occurring on the 1st day the cattle were introduced to the field and peak emissions occurring during the afternoon of the 2nd day. After 44 cattle had begun to graze the whole field during Period 2, peak emission rates occurred from 22–23 May, which is 2–3 days after the cattle had been introduced. A decreasing trend in emissions occurred after the cattle were removed from the field on 23 May until the end of the measurement period. This is in line with the reported emissions from urine and dung patches by Laubach et al. (2013a), where emissions peaked during the 3rd and 4th days after grazing had begun and a following decreasing trend in emissions after the cattle had been removed from the field on the 3rd day.

The peak in emissions which occurred during grazing can be attributed to the hydrolysis of urea within the urine patches, which leads to a rapid rise in pH and the formation of  $\text{NH}_4^+$  and a high rate of  $\text{NH}_3$  volatilisation (Sherlock and, Goh 1985). As volatilisation proceeds, a subsequent chemical reduction in surface pH occurs with an accompanying release of a proton to the transformation of  $\text{NH}_4^+$  to  $\text{NH}_3$  (Laubach et al., 2012; Sherlock and Goh, 1985; Móring et al., 2016), which prevents further volatilisation and can explain the declining emission rate after the cattle had left the field on 23 May.



#### 4.4 Emission factors from the grazing experiment

Emission factors from the grazing experiment have been evaluated as  $6 \pm 2$  and  $7 \pm 2$  g NH<sub>3</sub> cow<sup>-1</sup> day<sup>-1</sup> and  $9 \pm 3$  and  $10 \pm 3$  % of excreted urine-N emitted as NH<sub>3</sub> for the  $Q$  and  $Q_{\text{dep}}$  scenarios respectively (average emission factor  $\pm$  predicted  $C_b$  uncertainty). These emission factors were taken from the Period 2/Scenario 2 estimates as the measurements carried out during Period 1 did not capture the residual emissions which occurred after the cattle had left the field. The Period 1 and 2 emission estimates were derived from very different experimental conditions (particularly wetness and grazing density); therefore, we may not combine the two periods into a single emission factor. Previous experiments have measured NH<sub>3</sub> emissions from cattle urine patches at ratios of 7–25.7 % of excreted urine-N to grazed pastures (Jarvis et al., 1989; Ryden et al., 1987; Laubach et al., 2012, 2013a). Our estimates for emissions from grazing are towards the lower end of the range of published emission factors. Differences between reported emission factors may be related to differing weather conditions affecting the hydrolysis of urea or differences in soil properties, where emissions can be limited due to urine percolation into porous soil (Móring et al., 2016). It is also possible that significant emissions occurred after the miniDOAS instruments had been removed from the field, which would lead to an underestimation of the proportion of excreted N or urine-N emitted as NH<sub>3</sub>. The period of significant emissions from urine patches generally lasts 4–8 days after urine deposition (Sherlock and Goh, 1985; Laubach et al., 2012). However, a rainfall event after a dry period can lead to a delayed onset of NH<sub>3</sub> emissions by restarting urea hydrolysis (Móring et al., 2016). On the other hand, the Period 2 emission factors are also influenced to some degree by emissions from excretions during Period 1 on the SW field, which could cause an overestimation of emissions. Emission factors derived from Period 2 are also affected by  $u^*$  filtering, which may slightly increase estimates due to a measurement bias towards turbulent daytime periods.

The emission estimates presented here show that the gross emissions from the field ( $Q_{\text{dep}}$  scenario) are around  $16 \pm 6$  % higher than the net emissions ( $Q$  scenario). Both of these estimates are potentially useful to contribute towards an emission factor for livestock grazing. For example, regional-scale atmospheric dispersion models may require source inputs as gross emission factors due to deposition simulations implicit within the regional-scale model.

## 5 Conclusion

Fluxes of NH<sub>3</sub> were estimated through measurement of atmospheric concentrations upwind and downwind of a grazed field and the application of a bLS dispersion model to simulate the emission rate on a half-hourly ba-

sis from the observed horizontal concentration gradient and wind/turbulence measurements. The miniDOAS systems were well suited to the task, providing continuous high time resolution concentration measurements at field boundaries across the field. Horizontal concentration gradients of  $\sim 0$ – $9 \mu\text{g m}^{-3}$  were measured between upwind and downwind receptors. Control on emissions was observed from covariance with temperature, wind speed, and humidity and wetness measurements made on the field, revealing a diurnal emission profile. Two separate experiments to evaluate emissions were carried out: a Period 1 experiment (2 days) which took place on a small field with a grazing density of 44 cows ha<sup>-1</sup> and a Period 2 experiment (10 days) on a larger field with a grazing density of 22 cows ha<sup>-1</sup>. Spatial heterogeneity in emissions across the field was apparent during Period 2 because of uneven cattle distribution and a low grazing density, adversely affecting the accuracy of the bLS model estimates. However, after treating the larger field as a grid of discrete source areas, the spatial heterogeneity of emissions was accounted for by optimising source area coefficients to the measured concentrations and reconciling emission estimates between downwind receptors.

Data gaps in the  $C_b$  measurements were filled by applying linear regression equations with  $u$ ,  $T$  and RH, which introduced significant uncertainty into the emission estimates. The evaluated uncertainty in derived emissions due to  $C_b$  gap filling was 5 % during Period 1 and 31 % during Period 2.

In contrast to the standard bLS approach, we simulated the effect of redeposition to unsoiled field patches, where the canopy resistance ( $R_c$ ) component was estimated by an empirical model derived from local flux and  $R_c$  measurements with  $T$  and RH. Including deposition in the model increased emissions by  $16 \pm 6$  %. The results present both gross and net emissions from the field and show that deposition of NH<sub>3</sub> is an important consideration when deriving NH<sub>3</sub> emission factors.

**Data availability.** Data will be available at doi:10.5281/zenodo.576053 (Bell, 2016).

**Competing interests.** The authors declare that they have no conflict of interest.

**Acknowledgements.** This study was conducted as part of the French BtEP project (Emissions gazeuses au Bâtiment, sTockage, Epandage et Pâturage des systèmes bovins laitiers), convention no. 1360C0032, with funding provided by ADEME (Agence de l'environnement et de la maîtrise de l'énergie). We are thankful to the Région Bretagne regional council for PhD grant co-funding under the ARED scheme. We wish to thank David Sidaner, Jacques Lassalas and all of the staff at the INRA-Méjusseau dairy experimental farm. We wish to thank Andi Móring for assistance during the measurement campaign. We wish to thank

Thomas Kupper for organising the set-up of the N excretion model.

Edited by: H. Chen

Reviewed by: two anonymous referees

## References

- Asman, W. A. H.: Factors influencing local dry deposition of gases with special reference to ammonia, *Atmos. Environ.*, 32, 415–421, doi:10.1016/S1352-2310(97)00166-0, 1998.
- Asman, W. A. H., Sutton, M. A., and Schjorring, J. K.: Ammonia: emission, atmospheric transport and deposition, *New Phytol.*, 139, 27–48, doi:10.1046/j.1469-8137.1998.00180.x, 1998.
- Bell, M.: Dataset for article “Ammonia emissions from a grazed field estimated by miniDOAS measurements and inverse dispersion modelling”, doi:10.5281/zenodo.576053, 2016.
- Bracher, A., Schlegel, P., Munger, A., Stoll, W., and Menzi, H.: Moglichkeiten zur Reduktion von Ammoniakemissionen durch Futterungsmassnahmen beim Rindvieh (Milchkuh). Project report Schweizerische Hochschule fur Landwirtschaft und Agroscope Liebefeld-Posieux for the Swiss Federal Office of Agriculture, 128 pp., available at: <https://www.blw.admin.ch/blw/de/home/instrumente/ressourcen--und-gewaesserschutzprogramm/ressourcenprogramm.html> (last access: 4 October 2016), 2011.
- Bracher, A., Spring, P., Munger, A., Schlegel, P., Stoll, W., and Menzi, H.: Feeding measures to reduce ammonia emissions, *Proc. International Symposium on Emissions of Gas and Dust from Livestock (EMIL)*, 11–13 June 2012, Saint-Malo, France, edited by: Hassouna, M. and Guingand, N., p. 39, 2012.
- Carslaw, D. C. and Ropkins, K.: openair – An R package for air quality data analysis, *Environ. Modell. Softw.*, 27–28, 52–61, doi:10.1016/j.envsoft.2011.09.008, 2012.
- Erisman, J. W., Sutton, M. A., Galloway, J., Klimont, Z., and Winiwarter, W.: How a century of ammonia synthesis changed the world, *Nat. Geosci.*, 1, 636–639, doi:10.1038/ngeo325, 2008.
- Famulari, D., Fowler, D., Nemitz, E., Hargreaves, K. J., Storeton-West, R. L., Rutherford, G., Tang, Y. S., Sutton, M. A., and Weston, K. J.: Development of a low-cost system for measuring conditional time-averaged gradients of SO<sub>2</sub> and NH<sub>3</sub>, *Environ. Monit. Assess.*, 161, 11–27, doi:10.1007/s10661-008-0723-6, 2010.
- Felber, R., Munger, A., Neftel, A., and Ammann, C.: Eddy covariance methane flux measurements over a grazed pasture: effect of cows as moving point sources, *Biogeosciences*, 12, 3925–3940, doi:10.5194/bg-12-3925-2015, 2015.
- Flechard, C. R. and Fowler, D.: Atmospheric ammonia at a moorland site. I: The meteorological control of ambient ammonia concentrations and the influence of local sources, *Q. J. Roy. Meteor. Soc.*, 124, 733–757, doi:10.1002/qj.49712454705, 1998.
- Flechard, C. R., Fowler, D., Sutton, M. A., and Cape, J. N.: A dynamic chemical model of bi-directional ammonia exchange between semi-natural vegetation and the atmosphere, *Q. J. Roy. Meteor. Soc.*, 125, 2611–2641, doi:10.1002/qj.49712555914, 1999.
- Flechard, C. R., Spirig, C., Neftel, A., and Ammann, C.: The annual ammonia budget of fertilised cut grassland – Part 2: Seasonal variations and compensation point modeling, *Biogeosciences*, 7, 537–556, doi:10.5194/bg-7-537-2010, 2010.
- Flechard, C. R., Massad, R.-S., Loubet, B., Personne, E., Simpson, D., Bash, J. O., Cooter, E. J., Nemitz, E., and Sutton, M. A.: Advances in understanding, models and parameterizations of biosphere-atmosphere ammonia exchange, *Biogeosciences*, 10, 5183–5225, doi:10.5194/bg-10-5183-2013, 2013.
- Flesch, T. K., Wilson, J. D., and Yee, E.: Backward-Time Lagrangian Stochastic Dispersion Models and Their Application to Estimate Gaseous Emissions, *J. Appl. Meteorol.*, 34, 1320–1332, doi:10.1175/1520-0450(1995)034<1320:BtIsdm>2.0.Co;2, 1995.
- Flesch, T. K., Wilson, J. D., Harper, L. A., Crenna, B. P., and Sharpe, R. R.: Deducing ground-to-air emissions from observed trace gas concentrations: A field trial, *J. Appl. Meteorol.*, 43, 487–502, doi:10.1175/1520-0450(2004)043<0487:Dgefot>2.0.Co;2, 2004.
- Flesch, T. K., Wilson, J. D., Harper, L. A., and Crenna, B. P.: Estimating gas emissions from a farm with an inverse-dispersion technique, *Atmos. Environ.*, 39, 4863–4874, doi:10.1016/j.atmosenv.2005.04.032, 2005.
- Flesch, T. K., McGinn, S. M., Chen, D., Wilson, J. D., and Desjardins, R. L.: Data filtering for inverse dispersion emission calculations, *Agr. Forest Meteorol.*, 198, 1–6, doi:10.1016/j.agrformet.2014.07.010, 2014.
- Fowler, D., Pilegaard, K., Sutton, M. A., Ambus, P., Raivonen, M., Duyzer, J., Simpson, D., Fagerli, H., Fuzzi, S., Schjoerring, J. K., Granier, C., Neftel, A., Isaksen, I. S. A., Laj, P., Maione, M., Monks, P. S., Burkhardt, J., Daemmgen, U., Neirynck, J., Personne, E., Wichink-Kruit, R., Butterbach-Bahl, K., Flechard, C., Tuovinen, J. P., Coyle, M., Gerosa, G., Loubet, B., Altimir, N., Gruenhage, L., Ammann, C., Cieslik, S., Paoletti, E., Mikkelsen, T. N., Ro-Poulsen, H., Cellier, P., Cape, J. N., Horvath, L., Loreto, F., Niinemets, U., Palmer, P. I., Rinne, J., Misztal, P., Nemitz, E., Nilsson, D., Pryor, S., Gallagher, M. W., Vesala, T., Skiba, U., Brueggemann, N., Zechmeister-Boltenstern, S., Williams, J., O’Dowd, C., Facchini, M. C., de Leeuw, G., Flossman, A., Chaumerliac, N., and Erisman, J. W.: Atmospheric composition change: Ecosystems-Atmosphere interactions, *Atmos. Environ.*, 43, 5193–5267, doi:10.1016/j.atmosenv.2009.07.068, 2009.
- Gao, Z. L., Mauder, M., Desjardins, R. L., Flesch, T. K., and van Haarlem, R. P.: Assessment of the backward Lagrangian Stochastic dispersion technique for continuous measurements of CH<sub>4</sub> emissions, *Agr. Forest Meteorol.*, 149, 1516–1523, doi:10.1016/j.agrformet.2009.04.004, 2009.
- Genermont, S. and Cellier, P.: A mechanistic model for estimating ammonia volatilization from slurry applied to bare soil, *Agr. Forest Meteorol.*, 88, 145–167, doi:10.1016/S0168-1923(97)00044-0, 1997.
- Gill Instruments: Technical key note KN1509v3\* – software bug affecting “w” wind component notice and available options to customers – February 2016, available at: [http://gillinstruments.com/data/manuals/KN1509\\_WindMaster\\_WBug\\_info.pdf](http://gillinstruments.com/data/manuals/KN1509_WindMaster_WBug_info.pdf), last access: 4 October 2016.
- Hani, C.: bLSmodelR – An atmospheric dispersion model in R, R package version 2.4.1, available at: <http://www.agrammon.ch/documents-to-download/blsmodelr/>, last access: 22 September 2016.
- Hani, C., Sintermann, J., Jocher, M., and Neftel, A.: Ammonia emissions after application of slurry, 168 pp., Hochschule

- für Agrar-, Forst- und Lebensmittelwissenschaften, HAFL, Agroscope Institut für Nachhaltigkeitswissenschaften INH, available at: <http://www.agrammon.ch/assets/Downloads/SchlussberichtInklAnh20160728subm.pdf>, last access: 4 October 2016.
- Harper, L. A., Denmead, O. T., and Flesch, T. K.: Micrometeorological techniques for measurement of enteric greenhouse gas emissions, *Anim. Feed Sci. Tech.*, 166–167, 227–239, doi:10.1016/j.anifeedsci.2011.04.013, 2011.
- Hertel, O., Reis, S., Skjøth, C. A., Bleeker, A., Harrison, R., Cape, J. N., Fowler, D., Skiba, U., Simpson, D., Jickells, T., Baker, A., Kulmala, M., Gyldenkaerne, S., Sørensen, L. L., and Erisman, J. W.: Nitrogen processes in the atmosphere, in: *The European Nitrogen Assessment – Sources, Effects and Policy Perspectives*, edited by: Sutton, M. A., Howard, C. M., Erisman, J. W., Billen, G., Grennfelt, P., van Grinsven, H., and Grizzetti, B., Cambridge University Press, Cambridge, UK, 177–207, 2011.
- Hutchings, N. J., Sommer, S. G., Andersen, J. M., and Asman, W. A. H.: A detailed ammonia emission inventory for Denmark, *Atmos. Environ.*, 35, 1959–1968, doi:10.1016/S1352-2310(00)00542-2, 2001.
- Jarvis, S. C., Hatch, D. J., and Roberts, D. H.: The Effects of Grassland Management on Nitrogen Losses from Grazed Swards through Ammonia Volatilization – the Relationship to Excretal-N Returns from Cattle, *J. Agr. Sci.*, 112, 205–216, 1989.
- Kruit, R. J. W., van Pul, W. A. J., Sauter, F. J., van den Broek, M., Nemitz, E., Sutton, M. A., Krol, M., and Holtslag, A. A. M.: Modeling the surface-atmosphere exchange of ammonia, *Atmos. Environ.*, 44, 945–957, doi:10.1016/j.atmosenv.2009.11.049, 2010.
- Laubach, J., Taghizadeh-Toosi, A., Sherlock, R. R., and Kelliher, F. M.: Measuring and modelling ammonia emissions from a regular pattern of cattle urine patches, *Agr. Forest Meteorol.*, 156, 1–17, doi:10.1016/j.agrformet.2011.12.007, 2012.
- Laubach, J., Taghizadeh-Toosi, A., Gibbs, S. J., Sherlock, R. R., Kelliher, F. M., and Grover, S. P. P.: Ammonia emissions from cattle urine and dung excreted on pasture, *Biogeosciences*, 10, 327–338, doi:10.5194/bg-10-327-2013, 2013a.
- Laubach, J., Bai, M., Pinares-Patino, C. S., Phillips, F. A., Naylor, T. A., Molano, G., Rocha, E. A. C., and Griffith, D. W. T.: Accuracy of micrometeorological techniques for detecting a change in methane emissions from a herd of cattle, *Agr. Forest Meteorol.*, 176, 50–63, doi:10.1016/j.agrformet.2013.03.006, 2013b.
- Loubet, B., Cellier, P., Milford, C., and Sutton, M. A.: A coupled dispersion and exchange model for short-range dry deposition of atmospheric ammonia, *Q. J. Roy. Meteor. Soc.*, 132, 1733–1763, doi:10.1256/qj.05.73, 2006.
- Loubet, B., Asman, W. A. H., Theobald, M. R., Hertel, O., Tang, Y. S., Robin, P., Hassouna, M., Dammgén, U., Genermont, S., Cellier, P., and Sutton, M. A.: Ammonia Deposition Near Hot Spots: Processes, Models and Monitoring Methods, *Atmospheric Ammonia*, 205–267, doi:10.1007/978-1-4020-9121-6\_15, 2009.
- McGinn, S. M., Beauchemin, K. A., Flesch, T. K., and Coates, T.: Performance of a Dispersion Model to Estimate Methane Loss from Cattle in Pens, *J. Environ. Qual.*, 38, 1796–1802, doi:10.2134/jeq2008.0531, 2009.
- Menzi, H., Huguenin, O., Muenger, A., and Schlegel, P.: Procedure for defining new Swiss standard values for the nutrient excretions of dairy cows, in: *Proc. 16th RAMIRAN Conference*, 8–10 September 2015, Hamburg Harburg, Germany, edited by: Kormer, I., Lobkens, G., and Walk, S., Book of Abstracts, p. 52, 2015.
- Móring, A., Vieno, M., Doherty, R. M., Laubach, J., Taghizadeh-Toosi, A., and Sutton, M. A.: A process-based model for ammonia emission from urine patches, GAG (Generation of Ammonia from Grazing): description and sensitivity analysis, *Biogeosciences*, 13, 1837–1861, doi:10.5194/bg-13-1837-2016, 2016.
- Pain, B. F., Van der Weerden, T. J., Chambers, B. J., Phillips, V. R., and Jarvis, S. C.: A new inventory for ammonia emissions from UK agriculture, *Atmos. Environ.*, 32, 309–313, doi:10.1016/S1352-2310(96)00352-4, 1998.
- R Core Team: R: A language and environment for statistical computing, R Foundation for Statistical Computing, Vienna, Austria, available at: <https://www.R-project.org/>, last access: 4 October 2016.
- Reidy, B., Dammgén, U., Dohler, H., Eurich-Menden, B., van Evert, F. K., Hutchings, N. J., Luesink, H. H., Menzi, H., Misselbrook, T. H., Monteny, G. J., and Webb, J.: Comparison of models used for national agricultural ammonia emission inventories in Europe: Liquid manure systems, *Atmos. Environ.*, 42, 3452–3464, doi:10.1016/j.atmosenv.2007.04.009, 2008.
- Ryden, J. C., Whitehead, D. C., Lockyer, D. R., Thompson, R. B., Skinner, J. H., and Garwood, E. A.: Ammonia Emission from Grassland and Livestock Production Systems in the UK, *Environ. Pollut.*, 48, 173–184, doi:10.1016/0269-7491(87)90032-7, 1987.
- Sherlock, R. R. and Goh, K. M.: Dynamics of Ammonia Volatilization from Simulated Urine Patches and Aqueous Urea Applied to Pasture, 1. Field Experiments, *Fert. Res.*, 5, 181–195, doi:10.1007/Bf01052715, 1984.
- Sherlock, R. R. and Goh, K. M.: Dynamics of Ammonia Volatilization from Simulated Urine Patches and Aqueous Urea Applied to Pasture, 2. Theoretical Derivation of a Simplified Model, *Fert. Res.*, 6, 3–22, doi:10.1007/Bf01058161, 1985.
- Sintermann, J., Neftel, A., Ammann, C., Häni, C., Hensen, A., Loubet, B., and Flechard, C. R.: Are ammonia emissions from field-applied slurry substantially over-estimated in European emission inventories?, *Biogeosciences*, 9, 1611–1632, doi:10.5194/bg-9-1611-2012, 2012.
- Sintermann, J., Dietrich, K., Häni, C., Bell, M., Jocher, M., and Neftel, A.: A miniDOAS instrument optimised for ammonia field measurements, *Atmos. Meas. Tech.*, 9, 2721–2734, doi:10.5194/amt-9-2721-2016, 2016.
- Sommer, S. G., Sogaard, H. T., Moller, H. B., and Morsing, S.: Ammonia volatilization from sows on grassland, *Atmos. Environ.*, 35, 2023–2032, doi:10.1016/S1352-2310(00)00428-3, 2001.
- Sutton, M. A., Fowler, D., and Moncrieff, J. B.: The Exchange of Atmospheric Ammonia with Vegetated Surfaces, 1. Unfertilized Vegetation, *Q. J. Roy. Meteor. Soc.*, 119, 1023–1045, doi:10.1002/qj.49711951309, 1993.
- Sutton, M. A., Howard, C. M., Erisman, J. W., Bealey, W. J., Billen, G., Bleeker, A., Bouwman, A. F., Grennfelt, P., van Grinsven, H., and Grizzetti, B.: The challenge to integrate nitrogen science and policies: the European Nitrogen Assessment approach, in: *The European Nitrogen Assessment: Sources, Effects and Policy Perspectives*, edited by: Sutton, M. A., Howard, C. M., Erisman, J. W., Billen, G., Bleeker, A., Grennfelt, P., van Grinsven, H., and Grizzetti, B., Cambridge University Press, Cambridge, UK, 82–96, 2011.

- Tang, Y. S., Cape, J. N., and Sutton, M. A.: Development and Types of Passive Samplers for 570 Monitoring Atmospheric  $\text{NO}_2$  and  $\text{NH}_3$  Concentrations, *Sci. World*, 1, 513–529, doi:10.1100/tsw.2001.82, 2001.
- Volten, H., Bergwerff, J. B., Haaima, M., Lolkema, D. E., Berkhout, A. J. C., van der Hoff, G. R., Potma, C. J. M., Wichink Kruit, R. J., van Pul, W. A. J., and Swart, D. P. J.: Two instruments based on differential optical absorption spectroscopy (DOAS) to measure accurate ammonia concentrations in the atmosphere, *Atmos. Meas. Tech.*, 5, 413–427, doi:10.5194/amt-5-413-2012, 2012.
- von Bobruzki, K., Braban, C. F., Famulari, D., Jones, S. K., Blackall, T., Smith, T. E. L., Blom, M., Coe, H., Gallagher, M., Ghallaieny, M., McGillen, M. R., Percival, C. J., Whitehead, J. D., Ellis, R., Murphy, J., Mohacsi, A., Pogany, A., Junninen, H., Rantanen, S., Sutton, M. A., and Nemitz, E.: Field inter-comparison of eleven atmospheric ammonia measurement techniques, *Atmos. Meas. Tech.*, 3, 91–112, doi:10.5194/amt-3-91-2010, 2010.
- Wesely, M. L. and Hicks, B. B.: A review of the current status of knowledge on dry deposition, *Atmos. Environ.*, 34, 2261–2282, doi:10.1016/S1352-2310(99)00467-7, 2000.
- Whitehead, D. C.: *Grassland Nitrogen*, CAB International, Wallingford, UK, 1995.
- Zaman, M., Saggar, S., Blennerhassett, J. D., and Singh, J.: Effect of urease and nitrification inhibitors on N transformation, gaseous emissions of ammonia and nitrous oxide, pasture yield and N uptake in grazed pasture system, *Soil Biol. Biochem.*, 41, 1270–1280, doi:10.1016/j.soilbio.2009.03.011, 2009.